

A REVIEW: PREPARATION OF BISMUTH FERRITE NANOPARTICLES AND ITS APPLICATIONS IN VISIBLE-LIGHT INDUCED PHOTOCATALYSES

Tong Gao, Zhi Chen, Qiaoli Huang, Feng Niu, Xiani Huang, Laishun Qin and Yuexiang Huang

College of Materials Science and Engineering, China Jiliang University, No. 258 Xueyuan Street, Xiasha Higher Education District, Hangzhou 310018, Zhejiang Province, P.R. China

Received: April 11, 2014

Abstract. Photocatalyses such as hydrogen generation from water splitting or degrading organic contaminant on photocatalysts under solar light is promising in solving current energy and environmental issues. Bismuth ferrite (BiFeO_3) is a newly emerging photocatalytic material in parallel with the widely used TiO_2 -based materials, and the narrow band gap (2.1-2.7 eV) of BiFeO_3 -based materials (BFO) makes the visible-light photocatalysis such as hydrogen generation by water splitting become possible. In this review, BFO with different particle sizes and morphologies prepared by various preparation methods such as sol-gel, hydrothermal and microwave hydrothermal was summarized and the effects of particle size and/or morphology on the photocatalytic activity were discussed. The effects of the addition of dopants and formation of hetero-junction on the BFO photocatalytic activity were also evaluated. The examples of H_2 production and degradation of organic pollutants by using BFO as the photocatalysts were given in the end and the future work about the photocatalyses of BFO material is also suggested.

1. INTRODUCTION

The depletion of fossil fuel reserves vs. the continuously increasing energy demands and the corresponding environmental degradation on a world scale make the building of a clean and renewable energy utilization system be attractive at all time. Hydrogen as an energy or energy carrier may play an important role in such a system because its utilization process does not produce pollutants or greenhouse gases, particularly when the fuel cell is employed to use as a hydrogen energy converter. However, a wide use of hydrogen as a new energy is still facing many obstacles, namely the lack of naturally available diatomic H_2 though it is rich on earth as an element and the absence of efficient hydrogen storage technology. Currently, about 95% H_2 is produced by steam reforming of fossil fuels [1], which

consumes a large amount of energy and also produces pollutants or greenhouse gas such as nitrogen oxides and carbon oxides. Producing H_2 from water splitting reaction using solar energy as the primary energy source is promising because it may provide a potential solution for the dilemma of depletion of fossil fuel and environmental degradation. Ever since Fujishima et al. [2] discovered that the n-type TiO_2 photoelectrochemical (PEC) electrode can split water to generate hydrogen under irradiation of sunlight, much work has been done by using different types of semiconductors, such as ZnO [3,4], Fe_2O_3 [5], and WO_3 [6], as the photocatalysts in an attempt to photocatalytically produce H_2 from water splitting. Among them, TiO_2 is one of the mostly-investigated materials for photocatalytic hydrogen generation from water splitting due to its good chemi-

Corresponding authors: Z. Chen, e-mail: zchen0@gmail.com and Y. Huang, e-mail: yuexiang65@hotmail.com

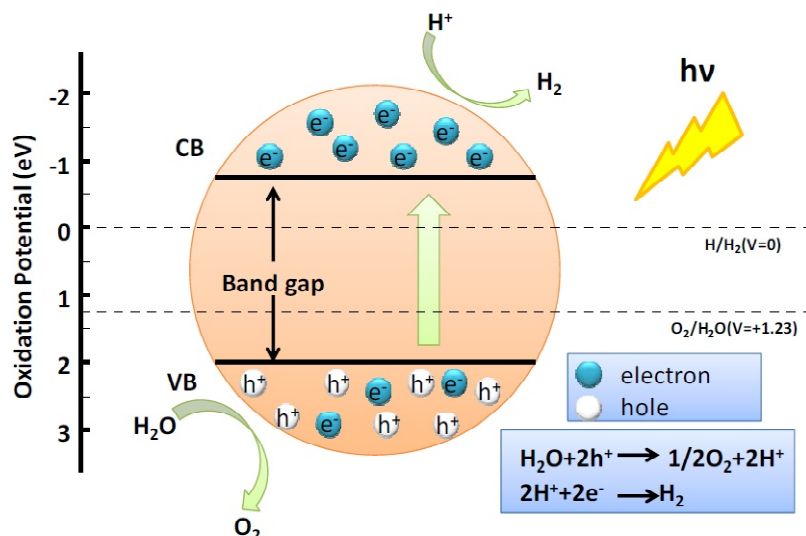
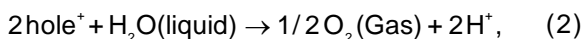


Fig. 1. Mechanism of hydrogen generation on semiconductor photocatalyst.

cal stability and easy availability [7]. The principle of photocatalytic water splitting to generate hydrogen on a semiconductor photocatalyst is schematically illustrated in Fig. 1 [8-10]. Incident light excites the intrinsic ionization over the band gap of n-type semiconducting material, which leads to the formation of electrons and holes in the semiconductor, Eq. (1). The holes split water molecules into O_2 and H^+ , Eq. (2). Simultaneously, the electrons generated in Eq. (1) reduce the H^+ into H_2 . The efficiency of water splitting is generally determined by the band gap, band structure and the electron transferring process.



Considering the potential of water splitting, the lowest energy of the absorbed photon must be larger than 1.23 eV to trigger this reaction. In view of the energy requirements set by H_2O reduction and oxidation potentials of the conduction band and valence band levels, the optimum band gap of semiconductor for efficient hydrogen production is about 2.0 eV. The photo-efficiency of water splitting on TiO_2 -based photocatalyst is greatly limited due to its large band gap (~ 3.2 eV) which restricts the absorption of visible light. This results in low quantum efficiency of hydrogen generation when these photocatalysts are used to split water under the visible light irradiation. Therefore, developing a new photocatalytic material that can directly split water into hydrogen under visible-light irradiation is essential for hydrogen pro-

duction; however, it is still a big challenge for both academic research and industrial application.

Bismuth ferrite ($BiFeO_3$ -type material) is a widely-known multiferroic material with simultaneously magnetic and electric ordering. Recently, bismuth ferrite has attracted a great of interests for solar applications due to its narrow band gap and the bulk photovoltaic effect [11,12]. Comparing with TiO_2 -based photocatalysts, $BiFeO_3$ has a narrower band gap of 2.1-2.7 eV, which allows the photocatalytic activity under visible light to become prominent. This is particularly important because visible-light energy occupies about 48% of the total solar energy; while UV light which is effective for TiO_2 -based photocatalysts only accounts for ca. 4% [12]. Bulk photovoltaic effect existing in materials without a center of symmetry such as ferroelectric materials has many unique features such as charge-carrier separation in a homogeneous medium, large photovoltage and a photocurrent proportional to the polarization magnitude [11-17]. The depolarization of electric field existing in $BiFeO_3$ -based materials may reduce the recombination of the photogenerated charged carriers during the transmission process [13-18]; which can further increase the quantum efficiency. Therefore, $BiFeO_3$ -based material can serve as a promising photocatalyst either for hydrogen generation from water splitting or for degradation of organic pollutants in the future.

In the present review, different methods for the syntheses of BFO ($BiFeO_3$ -type materials) with diverse morphologies such as nanoparticles [19], nanofibers [20], microcubes [21] and porous thin films [22] are summarized. The influence of morphology on the BFO photocatalytic activity is evalu-

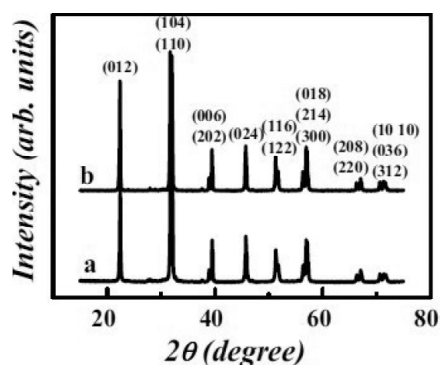


Fig. 2. XRD patterns of the BFO nanoparticles: (a) as-synthesized sample under the optimal conditions (500 °C for 2 h); (b) sample after the methyl orange degradation, reprinted with permission from F. Gao, X.Y. Chen, K.B. Yin, S. Dong, Z.F. Ren, F. Yuan, T. Yu, Z.G. Zou, J.M. Liu // *Adv. Mater.* **19** (2007) 2889-2892, (c) 2007 John Wiley and Sons.

ated. The recent progresses of photocatalytic application of BFO materials via water splitting are discussed. Examples of BFO as the photocatalysts are given in the end and the challenge of this material for further applications in photocatalytic hydrogen generation is also proposed.

2. PREPARATION OF BFO NANOPARTICLES

It is generally known that the particle size, morphology and crystallinity of a photocatalyst would significantly influence its photocatalytic activity. In recent years, various approaches such as sol-gel method [23], hydrothermal method [24], microwave hydrothermal method, solid state reaction [25,26] rapid liquid-phase sintering technique [27], pulsed laser deposition [28], electro-spinning [29], magnetron sputtering [30], and other methods [31,32] have been employed to obtain BFO particles with destined morphologies. The (sol-gel, hydrothermal and microwave hydrothermal method) details are discussed as follows.

2.1. Sol-gel method

To obtain well-crystallized, pure perovskite bismuth ferrite nanoparticles, sol-gel process is intensively used to synthesize BFO because it can easily achieve a uniform composition on molecular level and at a relative low synthesis temperature. Gao et al. reported that single-phase BiFeO₃ particles with a perovskite structure and a size ranging from 80 nm to 120 nm were obtained by a sol-gel method using Fe(NO₃)₃·9H₂O and Bi(NO₃)₃·5H₂O dissolved

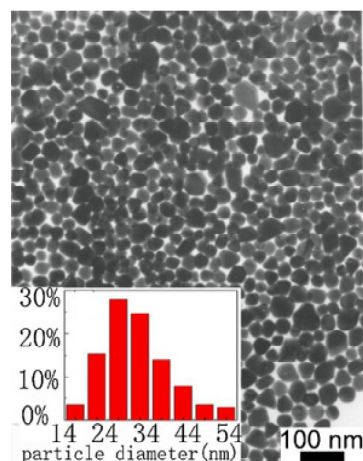


Fig. 3. TEM micrograph of the prepared BiFeO₃ nanoparticles and the histogram of size distribution (inset), reprinted with permission from X. Wang, Y. Lin, X.F. Ding, J.G. Jiang // *J. Alloys and Compounds.* **509** (2011) 6585, (c) 2011 Elsevier.

in glycol as the precursors [19], as shown in Fig. 2. Wang et al. also synthesized multiferroic BiFeO₃ nanoparticles with a particle size ranging from 35 to 90 nm by a glycol-based sol-gel route and the synthetic temperature was lowered to 500 °C [33,34]. The TEM micrograph shown in Fig. 3 illustrates that the as-prepared BiFeO₃ particles are in a quasi spherical shape. Yang et al. reported a sol-gel route in an attempt to control the size of BiFeO₃ nanoparticles [35]. Their results showed that the grain size of BiFeO₃ particles could be tailored by changing the composition ratio between acrylamide and bisacrylamide. The average grain size from 52 nm to 110 nm identified by Debye-Scherrer formula was attained in their work [36]. In general, sol-gel method is a simple way to synthesize BiFeO₃ nanoparticle. However, the processing parameters should carefully be controlled so as to obtain the required crystalline phase, morphology as well as particle size.

2.2. Hydrothermal method

Hydrothermal method is also used to synthesize BiFeO₃ nanoparticles by many researchers [37-45]. Comparing with sol-gel process in which a relative high temperature, e.g. 500 °C, is needed to calcine the gel for obtaining BFO, the hydrothermal method can directly synthesize BFO at a relatively low temperature. It offers an opportunity to better control the purity, morphology and size of BFO material. Peng et al. reported that a single-phase BiFeO₃ was synthesized by a hydrothermal method [37]. In their work, FeCl₃ and Bi(NO₃)₃·5H₂O were

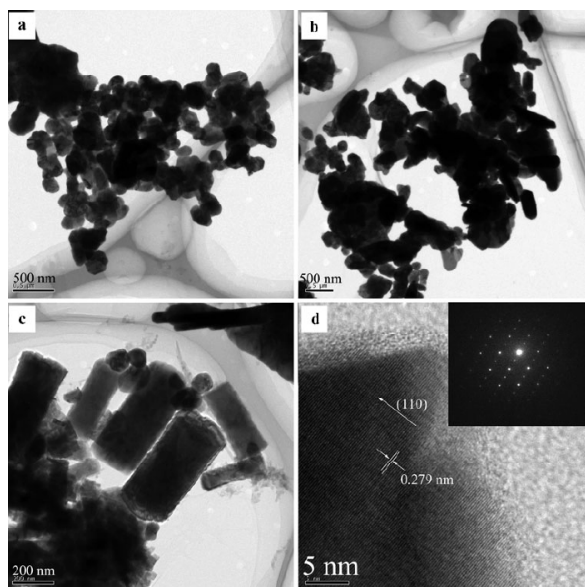


Fig. 4. TEM micrographs of the BFO powders synthesized at 170 °C for 16 h using different NaOH concentrations: 0.03 M (a), 0.07 M (b), 0.10 M (c); (d) HRTEM micrograph of the rod-like BFO particles and SAED pattern (inset), reprinted with permission from J.H. Peng, M. Hojamberdiev, B.W. Cao, J.A. Wang, Y.H. Xu // *Applied Physics a-Materials Science & Processing*. **103** (2011) 511, (c) 2011 Elsevier.

used as the starting materials and the hydrothermal experiments were carried out at a temperature range of 150-190 °C with a NaOH concentration range of 0.03-0.12 M. Pure BiFeO₃ could be obtained by

selecting appropriate hydrothermal parameters such as reaction temperature, reaction time and NaOH concentration. Especially, it is interesting to note that different morphologies of BiFeO₃ particles were obtained by varying NaOH concentrations during the hydrothermal synthesis process, as shown in Fig. 4. When a low NaOH concentration of 0.03 M was used, the as-prepared BFO particles were irregular with an averaged particle size around 250 nm, as shown in Fig. 4a. Some rod-like particles with a size of 250 nm in width and 400 nm in length (Fig. 4b) were formed when NaOH concentration was increased to 0.07 M. When NaOH concentration was further increased to 0.10 M, most BFO particles were in a rod-like shape with the maximum length of 500 nm (Fig. 4c). The HRTEM image of the rod-like particle, as shown in Fig. 4d, indicates that submicron particle is single crystalline with interplanar spacing of about 0.28 nm, which corresponds to the (110) crystalline plane of the hexagonal phase BFO bulk crystal. The SAED pattern (the inset of Fig. 4d) taken from the rod-like particle further confirms that the observed BFO particle is single crystalline. The detailed results of hydrothermal parameters on the formation of BiFeO₃ powders are listed in Table 1. Zhou et al. also carried out a similar processing to synthesize BiFeO₃ particles by using KOH to replace NaOH [38]. They also realized the morphology control of BiFeO₃ by changing KOH concentration. It was observed that the morphology of synthesized BiFeO₃ changed from irregular ag-

Table 1. The influences of the processing parameters on the formation of BiFeO₃ powders, see [37], (reprinted with permission from J.H. Peng, M. Hojamberdiev, B.W. Cao, J.A. Wang, Y.H. Xu // *Applied Physics a-Materials Science & Processing*. **103** (2011) 511, (c) 2011 Elsevier).

| NaOH Concentration, (M) | Time, (h) | Temperature, (°C) | Formed crystal phase |
|-------------------------|-----------|-------------------|----------------------------------------------------------------------------------------------------------|
| 0.01 | 16 | 170 | Bi ₂ Fe ₄ O ₉ , BiFeO ₃ |
| 0.03 | 16 | 170 | BiFeO ₃ |
| 0.07 | 4 | 170 | Bi ₂ Fe ₄ O ₉ , BiFeO ₃ |
| 0.07 | 6 | 170 | BiFeO ₃ |
| 0.07 | 10 | 170 | BiFeO ₃ |
| 0.07 | 16 | 140 | Bi ₂₅ FeO ₄₀ , BiFeO ₃ |
| 0.07 | 16 | 150 | BiFeO ₃ |
| 0.07 | 16 | 170 | BiFeO ₃ |
| 0.07 | 16 | 190 | BiFeO ₃ |
| 0.07 | 16 | 200 | Bi ₂ Fe ₄ O ₉ , BiFeO ₃ |
| 0.07 | 20 | 170 | BiFeO ₃ |
| 0.10 | 16 | 170 | BiFeO ₃ |
| 0.12 | 16 | 170 | BiFeO ₃ |
| 0.15 | 16 | 170 | Bi ₂ Fe ₄ O ₉ , BiFeO ₃ |
| 0.20 | 16 | 170 | Bi ₂ Fe ₄ O ₉ , BiFeO ₃ , Bi ₂₅ FeO ₄₀ |

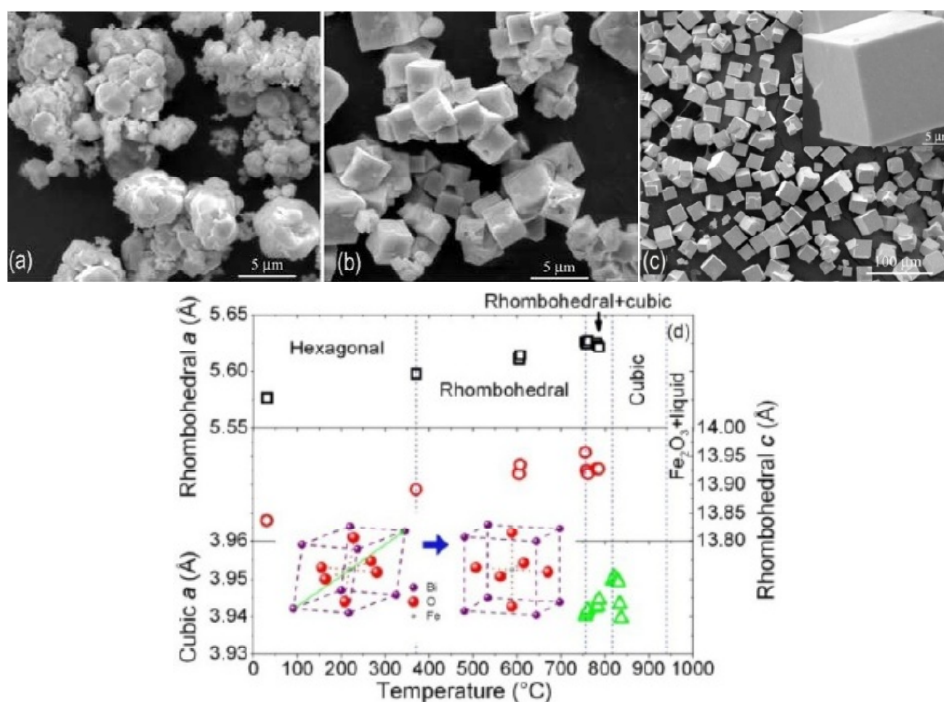


Fig. 5. SEM micrograph of BiFeO_3 powders synthesized at 200 °C for 4 h using different KOH concentrations: 4 M (a), 6 M (b) and (c) 7 M; (d) the phase transition of BiFeO_3 prepared by hydrothermal method, reprinted with permission from J.P. Zhou, R.L. Yang, R.J. Xiao, X.M. Chen, C.Y. Deng // *Mater. Res. Bull.* **47** (2012) 3630, (c) 2012 Elsevier.

glomerations to regular cubes (about 20 nm size with smooth surfaces) when KOH concentration was increased from 4 M to 7 M, as shown in Fig. 5. The formation of different morphologies was explained by the electric charge effect (the growth of polyhedral particles along different directions with different rates due to the specific surface energy can be affected by the concentration of KOH) on the surfaces of BiFeO_3 particles. Fig. 5d demonstrates the proposed crystal structure transition of BiFeO_3 cubic micro-particles. Jiang et al. investigated the influence of dispersant, mineralizer and solvent on the morphology, particle size and agglomeration of BiFeO_3 prepared by a hydrothermal route [39]. In their work, wafer-like BiFeO_3 particles with an average diameter of 100-500 nm could be obtained by a hydrothermal process without dispersant or mineralizer. However, the morphology of the as-prepared BFO particles is different when dispersant or mineralizer was added. As shown in their report, well-dispersed BFO microsphere with the uniform diameter of about 50 nm could be synthesized by using PEG 200 as dispersant which is constituted by a sheet of porous spherical. As for preparation by using KNO_3 as a mineralizer, the obtained BFO particles are spindle-like agglomeration with an average diameter of ~2 μm . However, very beautiful flower-like shape BFO could be synthesized by employing etha-

nol as the solvent and nano-spherical particles of ~20 nm size are also observed on the flower petal. Such differences in morphology, size and agglomeration are ascribed to the consequence that the presence of dispersant, mineralizer and solvent would affect the BFO formation kinetics during hydrothermal process.

BFO particles with diverse morphologies such as irregular particles [40], wafer-like particles [38], nanowires [41,42], tubes [43,44], spheres, cubes [21,45] could be obtained by the hydrothermal process. It seems that the grain size and morphology of BiFeO_3 can be better controlled by this processing, though the reported particle size is larger than those prepared by the sol-gel method.

2.3. Microwave hydrothermal method

Microwave hydrothermal method is another promising technique which introduces microwave heating into the hydrothermal process. It allows the reaction system to be rapidly heated to the crystallization temperature (about 1-2 orders of magnitude comparing with the conventional hydrothermal process), and thus can greatly reduce the reaction time. This is particularly important when production efficiency and composition homogeneity have to be taken into account [46,47].

Recently, microwave hydrothermal method has been introduced to synthesize perovskite bismuth ferrite nanomaterials. Komarneni et al. first reported the synthesis of highly crystalline BiFeO_3 at 194°C using the microwave hydrothermal process [48]. However, the as-prepared BFO materials were found to be heavily aggregated. Joshi et al. obtained single-crystalline BiFeO_3 nanocubes with a size of 50–200 nm by heating at 180°C for 30 min under microwave hydrothermal process [45]. Particle agglomeration was also observed in the acquired products. Tan et al. reported that pure-phase BiFeO_3 , pure-phase $\text{Bi}_{25}\text{FeO}_{40}$ and the mixture of $\text{Bi}_{25}\text{FeO}_{40}$ and BiFeO_3 could be prepared through a microwave hydrothermal method by tuning the temperature and KOH concentration [46]. The three kinds of BFO materials (BiFeO_3 , $\text{Bi}_{25}\text{FeO}_{40}$, and mixture of $\text{Bi}_{25}\text{FeO}_{40}$ and BiFeO_3) demonstrated different morphology, crystallinity, specific surface areas and accordingly distinct differences in photocatalytic activity. The influence of temperature on the morphology of the BFO materials is illustrated in Fig. 6. It is clearly seen that the particles were almost irregular (Figs. 6a and 6b) when the reaction tem-

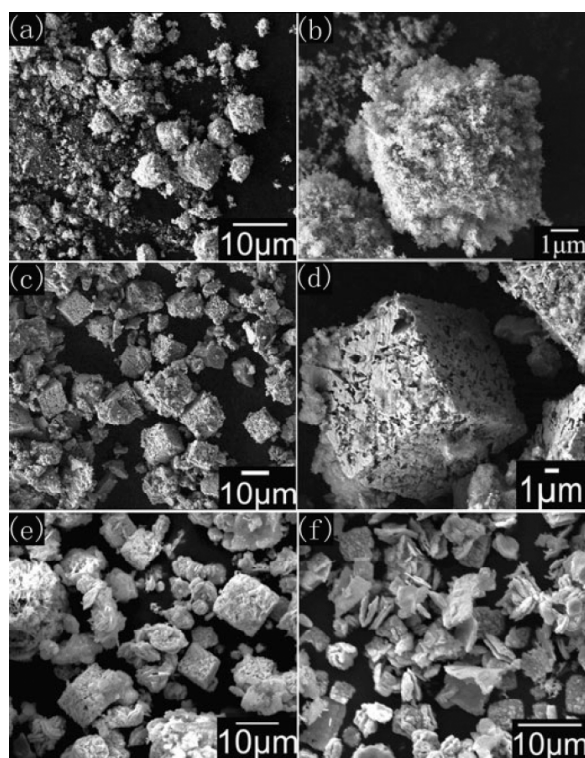


Fig. 6. SEM micrograph of BFO powders synthesized with KOH concentration of 0.5 M: (a) and (b) 160°C ; (c) and (d) 180°C ; (e) 190°C ; (f) 200°C , reprinted with permission from G.Q. Tan, Y.Q. Zheng, H.Y. Miao, A. Xia, H.J. Ren // *J. Am. Ceram. Soci.* **95** (2012) 280, (c) 2012 John Wiley and Sons.

perature was below 180°C . The particles were in a porous cube-like shape when the reaction temperature was increased to 180°C , as shown in Figs. 6c and 6d. Mussel-like particles began to form when the reaction was increased to 190°C (Fig. 6e). When the temperature was further increased to 200°C , only mussel-like particles were observed since the dissolve-recrystallization process was believed to be predominant (Fig. 6f). Zhu et al. synthesized two types of bismuth ferrite by using $\text{Fe}(\text{NO}_3)_3 \cdot 9\text{H}_2\text{O}$ and $\text{Bi}(\text{NO}_3)_3 \cdot 5\text{H}_2\text{O}$ as original materials. One was spherical perovskite-type bismuth ferric nanocrystals with diameters of 10–50 nm, as shown in Fig. 7a; and the other was hexagonal-shaped sillenite-type bismuth ferritic nanocrystals with sizes of 18–33 nm, as shown in Fig. 7b [47]. The results of Rh B ($\text{C}_{28}\text{H}_{31}\text{ClN}_2\text{O}_3$) photodegradation indicated that the sillenite-type bismuth ferritic nanocrystals with a hexagonal shape and size of 18–33 nm showed a higher photocatalytic activity than the spherical perovskite-type BiFeO_3 nanocrystals. The higher photocatalytic activity has been ascribed to the smaller average particle size and the unique hexagonal morphology of sillenite-type compound.

From the above discussion, it can be concluded that microwave hydrothermal method is an appropriate route to obtain homogeneous nanosized bismuth ferric in a short time.

2.4. Other synthetic methods

In addition to the above mentioned preparation methods, other synthetic methods were also employed to prepare BFO nanomaterials. A facile block copolymer-directed synthetic process was reported by

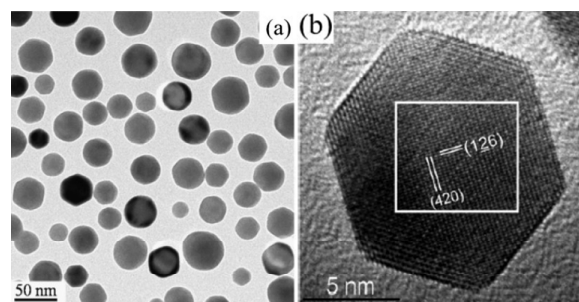


Fig. 7. (a) TEM micrograph of a single BiFeO_3 nanocrystal with a diameter of ~ 12 nm. (b) HRTEM micrograph of a single sillenite-type bismuth ferritic nanocrystal with a particle size of 13 nm, reprinted with permission from X.H. Zhu, Q.M. Hang, Z.B. Xing, Y. Yang, J.M. Zhu, Z.G. Liu, N.B. Ming, P. Zhou, Y. Song, Z.S. Li, T. Yu, Z.G. Zou // *J. Am. Ceram. Soci.* **94** (2011) 2688, (c) 2011 John Wiley and Sons.

Reitz et al. [49]. They obtained rhombohedral BiFeO_3 thin films which showed a mesoporous nanocrystalline framework [50]. Hengky et al. achieved the BiFeO_3 nanoparticles using a self-combustion method [51,52]. Wang et al. synthesized pure-phase BiFeO_3 powders with micron-sized porous structure and nano-sized particle structure by direct thermal decomposition of metal nitrates at 500 °C [53]. Wang et al. fabricated BiFeO_3 nanofibers via a facile electrospinning technique combining with sol-gel method [54]. Yang et al. reported the combustion-method synthesis of single-phase and well-crystallized BiFeO_3 at a low temperature of 300 °C [55]. Fei et al. utilized a facile and controllable route to synthesize pure-phase BiFeO_3 pills, cubes and rods with highly exposed $\{111\}_c$ facets [56]. The BiFeO_3 microstructures of pills (Figs. 8a and 8b), cubes (Figs. 8c and 8d), and rods (Figs. 8e and 8f) are shown in Fig. 8.

It can be summarized that BiFeO_3 with different grain sizes and diverse morphologies may be prepared by using different preparation methods and/or by altering processing parameters. The effects of synthetic methods on the characteristics of bismuth ferrite particles are listed in Table 2. The influence of particle characteristics on the photocatalytic properties of BiFeO_3 will be discussed in a later section.

3. FACTORS AFFECT THE PHOTOCATALYTIC ACTIVITY OF BFO PARTICLE

Since Ramesh et al. [12] discovered the bulk photovoltaic effect of BFO material, much work has been done on its photovoltaic related applications [57-62]. The relative narrow band-gap (2.1-2.7 eV) BFO material allows the absorption of sunlight extended up to 750 nm. Thus, the applications of BFO materials either in degradation of pollutants or in photo-

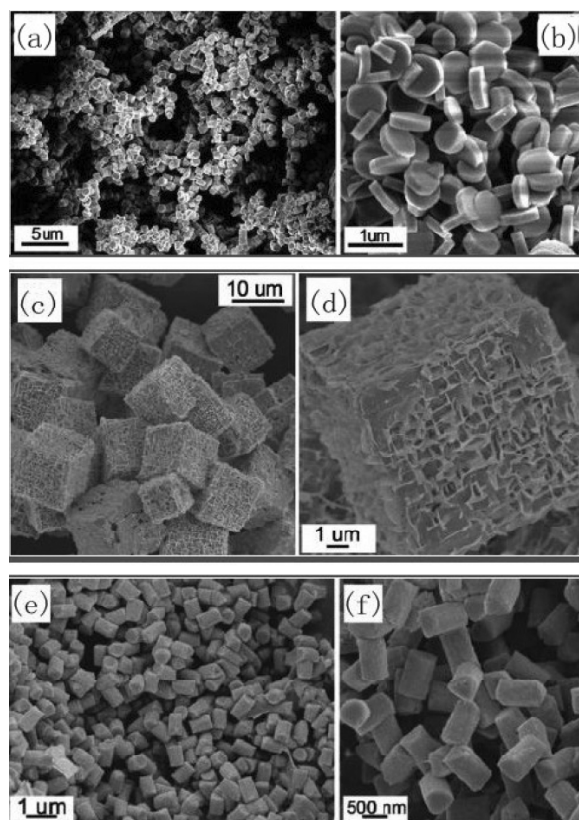


Fig. 8. SEM micrograph of different morphology BFO: (a) Low magnification and (b) high magnification of pills; (c) Low magnification and (d) high magnification of cubes; (e) Low magnification and (f) high magnification of rods, reprinted with permission from L. Fei, J. Yuan, Y. Hu, C. Wu, J. Wang, Y. Wang // *Crystal Growth & Design*. **11** (2011) 1049, (c) 2011 American Chemical Society.

catalytic hydrogen generation from water splitting under visible light have attracted much attention [63]. For instance, the RhB dye in industrial wastewater could be completely degraded under direct sunlight irradiation for 35 min by using BiFeO_3 as the photo-

Table 2. The preparation method of bismuth ferrite.

| Synthesis method | Conditions | Grain size (nm) | Morphology | Ref. |
|------------------|----------------|-----------------|---------------------|------------|
| Sol-gel | Calcination | ~20 | spherecube, | [33,34] |
| Hydrothermal | No calcination | ~200 | pill, Waferhexagon, | [37,38,44] |
| Microwave | No calcination | ~50 | sphereordered | [46,48] |
| hydrothermal | | | | |
| Self-assembled | Annealing | ~100 | network | [49] |
| Self-combustion | 300 °C | ~50 | hexagon | [51,52] |
| Thermal | 500 °C | ~80 | irregular particle | [53] |
| decomposition | | | | |
| Electrospinning | Annealing | ~300 (diameter) | fiber | [54] |
| technique | | | | |

catalyst [64]. Some researchers [65,66] were also involved in using BFO materials to generate hydrogen through water splitting from a photocatalytic or photoelectrochemical (PEC) process, though the mechanism is still not well understood.

It is recognized that many factors may have influences on the photocatalytic efficiency of a given material. For instance, the particle size, morphology as well as dopants could significantly affect hydrogen evolution capability of a certain photocatalyst during the photocatalytic process. Some modifications such as doping [67] and sensitization [68] are used to enhance the photocatalytic performances of hydrogen production.

3.1. Photocatalytic mechanism of BFO nanoparticles

As discussed above, the photocatalytic hydrogen generation from water splitting on a semiconductor-type photocatalyst such as TiO_2 follows a mechanism illustrated in Fig. 1. The photo-induced electron holes split water molecules into O_2 and H^+ ; while hydrogen ions are reduced into H_2 by the photogenerated electrons. It is well known that the visible-light response and the separation of photogenerated electron-hole pair are two key factors for the photocatalytic performance under solar irradiation. As the above discussions, BFO can have a better visible-light response since it poses a narrower band gap comparing with that of TiO_2 . Moreover, BFO may have a high separation efficiency of the photogenerated electron and hole due to the self-polarization field caused by self-polarization in ferromagnetic materials [69-71]. However, the actual mechanism for the separation of photogenerated electron and hole in ferroelectrics is disputable and a deeper understanding is essential; although the research for this field started 30 years ago [54,70-72].

3.2. Effect of particle morphology

It is known that the photocatalytic performance would be largely dependent on the morphology of synthesized particles. Many efforts have been made to realize morphology control over obtained BFO particles for achieving better photocatalytic properties. Fei et al. reported that pills and rods with highly exposed $\{111\}_c$ showed an enhanced visible-light response in comparison with $\{100\}_c$ dominant cubes [55]. Different photocatalytic activities from different crystal facets were also observed by Cai et al. [73]. Such a difference is attributed to the different sur-

face energy levels of the conduction and valence bands from different crystal facets. Zhang et al. also reported that the photocatalytic properties of bismuth ferrite nanoparticles in the UV and visible light range largely depended on the morphology of the crystals, and the sequence of catalytic activity under the visible light was cube > plate > sheet [74]. Wang et al prepared BiFeO_3 nanoparticles by using a sol-gel method and found that the morphology and surface area had remarkably influence on the photocatalytic activities under visible light, their report showed that the photocatalytic activity of BiFeO_3 nanoparticles were better than the BiFeO_3 bulk [33]. Zhu et al. reported that the hexagonal-shaped BFO morphology showed a better photocatalytic activity than the spherical perovskite-type BFO [47].

It can be concluded that a BiFeO_3 particle with $\{100\}_c$ dominant cube has preferable photocatalytic activity prepared by hydrothermal method. If a hexagonal-shaped BFO particle which prepared by sol-gel method has bigger surface area should be showed a better photocatalytic performance.

3.3. Effect of dopants

Introducing dopants into the lattice of photocatalysts is generally used to adjust the band gap of semiconductors. As for BFO material, the band structure can be altered by introducing an intermediate energy level inside the band gap and/or changing the band gap itself. In addition to the theoretical work, considerable experimental efforts have also been made to alter the band structure of BiFeO_3 by doping. The acquired experiments indicated that the photocatalytic performance could be significantly enhanced by doping. Mukherjee et al. reported that rare earth transition metal was an effective dopant and that the electronic band structure of BiFeO_3 could be tuned by the addition of Y (BYFO) or La [75]. The band gap of BFO is expanded with the addition of Y and increased with the increase of the amount of Y. Whereas, the band gap decreased with the addition of rare earth transition metals such as La [76]. Zhang et al. investigated the influence of La doping on the crystal structure and the photoabsorption tests revealed that doping with La had little influence on the optical property [77]. Mukherjee et al. reported the band gap of the prepared BiFeO_3 and BYFO nanoparticles varied from 2.0 to 2.3 eV and the doped BYFO had higher photocatalytic properties than those of BiFeO_3 [78].

The dopant can replace metal cations on the original sites which results in the lattice substitution. However, as for the photocatalytic application,

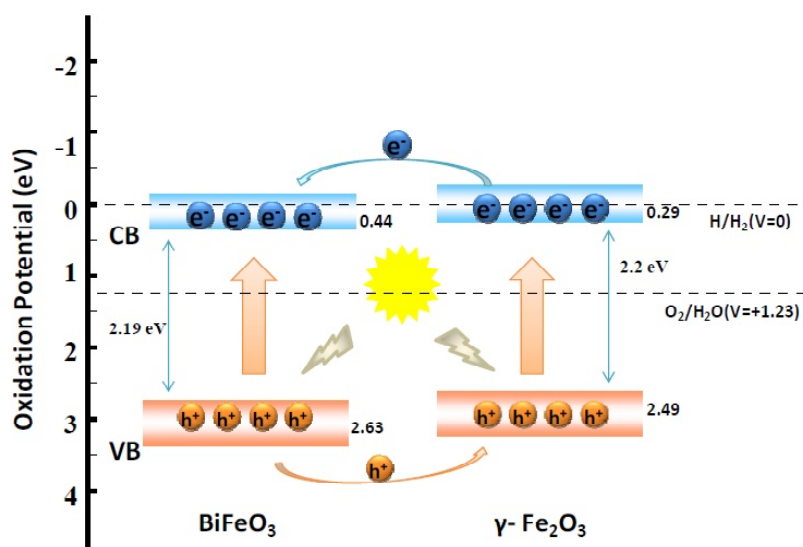


Fig. 9. Schematic illustration of the calculated energy-level diagram of BFO- Fe_2O_3 heterojunction, reprinted with permission from R. Guo, L. Fang, W. Dong, F. Zheng, M. Shen // *J. Mater. Chem.* **21** (2011) 18645, (c) 2011 Royal Society of Chemistry.

doping is sometimes regarded as an unsuitable method since the dopant can also serve as a new recombination center for photo-generated electrons and holes. Anyway, doping can be an effective method if suitable doping elements are selected.

3.4. Effect of hetero-junction

The effective separation of photo-generated electrons and holes is also essential to improve photocatalytic activity of semiconductors. The formation of a hetero-junction from two kinds of materials is generally believed to be effective on enhancing the photocatalytic activity due to the reduced recombination rate of photogenerated electrons and electron holes [79-82]. In the case of BFO materials, Fe_2O_3 is sometimes selected to form a hetero-junction with BFO. Since both BFO and Fe_2O_3 can be excited by visible light even they have different photo-absorption ranges, the photocatalytic reaction is initiated by the absorption of visible-light photons with energy equal to or higher than the band gap in either BFO or Fe_2O_3 semiconductors. This results in the creation of electrons and photogenerated holes in the valence band (VB) and conduction band (CB), respectively. According to the band edge position, the excited electrons in the CB of BFO transfer to the CB of Fe_2O_3 ; simultaneously, the holes in the VB of Fe_2O_3 can move to VB of BFO due to the potential difference of the band energy. Therefore, the recombination of electron and hole can be restricted and the corresponding photocatalytic activity is accordingly enhanced. The energy band diagram of BFO/ Fe_2O_3 is shown in Fig. 9. Guo et al.

synthesized BFO nanoparticles mixed with a parasitic Fe_2O_3 phase by using sol-gel method [83]. BFO/ Fe_2O_3 composite with an optimal ratio between the two phases of BFO and Fe_2O_3 showed an improved photocatalytic activity, which was ascribed to the formation of a BFO/ Fe_2O_3 hetero-junction. It is obvious that the formation of a hetero-junction is efficient way to enhance the photocatalytic performance of BFO.

In addition to the above factors from photocatalysts, the experimental parameters also have influences on the photocatalytic activities. Wang et al. found that BiFeO_3 nanoparticles could have a higher photocatalytic activity in the solution with a lower pH value [34]. The photocatalytic activity could be enhanced by increasing the surface area of the prepared films [22]. Wang et al. reported that H_2O_2 could enhance the photocatalytic activities of BiFeO_3 [33]. Li et al. reported a facile method of preparing reduced graphene (RGO)- BiFeO_3 nanocomposite through self-assembly and found that the magnetic and optical performances of this nanocomposite could be enhanced due to the interaction between RGO and BiFeO_3 [85].

4. PHOTOCATALYTIC APPLICATIONS OF BFO PARTICLES

4.1. Degradation of organic pollutants on BFO particles

In recent year, many experiments have shown that bismuth ferrite can effectively degrade organic pollutants. Gao et al. have used ~ 120 nm BiFeO_3

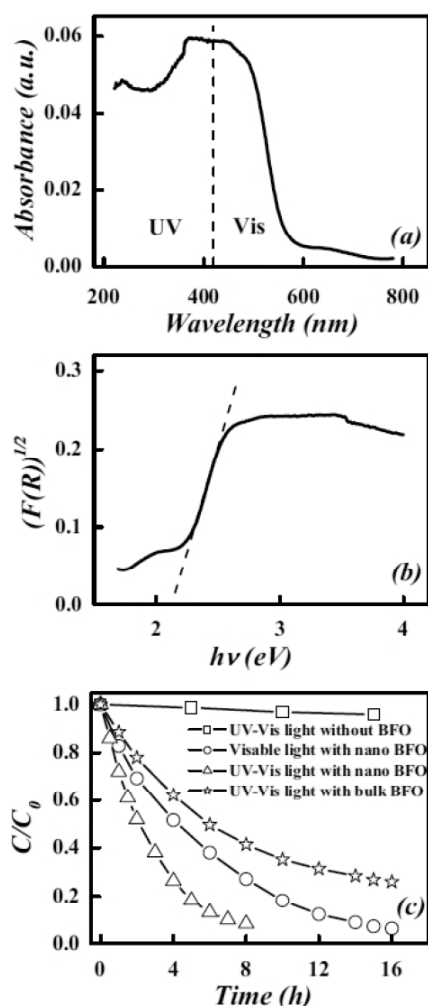


Fig. 10. (a) UV-vis diffuse reflectance spectrum of the BiFeO_3 nanoparticles, where the dot line is the division between UV and visible light; (b) the square root of Kubelka-Munk functions $F(R)$ versus photon energy, where the dot line is tangent of the linear part; (c) photocatalysis of BiFeO_3 nanoparticles and bulk on degradation of methyl orange under UV-vis light irradiation and visible light irradiation, reprinted with permission from R. Guo, L. Fang, W. Dong, F. Zheng, M. Shen // *J. Mater. Chem.* **21** (2011) 18645, (c) 2011 Royal Society of Chemistry.

nanoparticles to degrade methyl orange (MO) under visible light and almost all of the methyl orange was degraded after 16 h, as shown in Fig. 10 [19]. In the report of Wang et al., the BiFeO_3 nanoparticles with the average particle size of 35 nm could successfully degrade RhB within 1 h [34]. The experiment of Jiang et al. proved that BiFeO_3 could effectively degrade methylene blue under visible-light irradiation [39]. Xu et al. reported that in the visible light irradiation BiFeO_3 could degrade Congo red, although the degradation effect is not so good [22]. These results predict that BiFeO_3 may have the promising applications in water treatment.

4.2. Photocatalytic H_2 generation on BFO particles

Deng et al. carried out H_2 generation from water on BiFeO_3 nanoparticles [63]. The experimental device is given in Fig. 11a. The photocatalytic activity of H_2 production from water splitting on BiFeO_3 was operated under AM 1.5 (air mass) conditions. Fig. 11b shows the H_2 generation reaction using BiFeO_3 as the photocatalyst in 1 M KOH, red line is the result from P25 titania photocatalyst. The amount of H_2

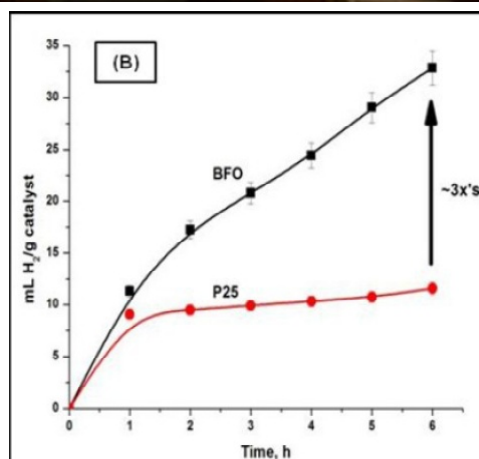
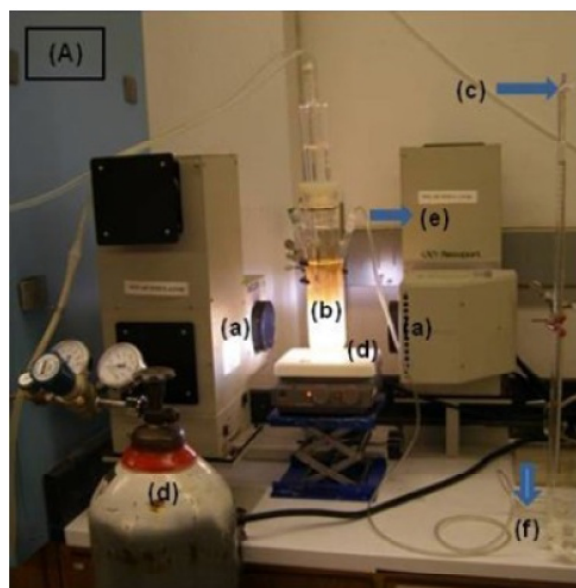


Fig. 11. (A) Photocatalytic H_2 generation system using BFO as a catalyst in 1(M) KOH; (a) solar simulator light source, (b) reactor, (c) burette for collecting gas by downward displacement of water, (d) N_2 cylinder for purging, (e) gas collection outlet, (f) petridish containing water; (B) Volume versus time graph showing the volume of H_2 evolved during the photocatalytic splitting of water, reprinted with permission from J. Deng, S. Banerjee, S.K. Mohapatra, Y.R. Smith, M. Misra // *J. Fundamentals of Renewable Energy and Applications.* **1** (2011) 1, (c) 2011 Royal Society of Chemistry.

generated on BiFeO₃ was 34 cm³·g⁻¹ after 6 h of illumination which was nearly three times of that on P25 photocatalyst. The higher photocatalytic activity was ascribed to the positive absorption in the visible light and the efficient charge separation on BiFeO₃ material. Up to now, few reports about photocatalytic H₂ generation on BiFeO₃ nanoparticles and further research is made in many aspects.

5. SUMMARY AND OUTLOOK

This review gives an overview on the preparation of BiFeO₃ nanoparticles and their potential application in photocatalyses such as hydrogen generation from water splitting or degrading organic contaminant. Focus was placed on the preparation methods to achieve controllable particle size and morphology which should affect the photocatalytic properties. BFO particles with diverse sizes and morphologies prepared by various preparation methods such as sol-gel, hydrothermal and microwave hydrothermal were summarized and the effects of particle size and morphology on the photocatalytic activity, particularly on photocatalytic hydrogen generation from water splitting and degrading organic contaminant, were discussed. It was concluded that the photocatalytic activity of BFO is related with the particle size and morphology, BiFeO₃ particle with {100}_c dominant cube showed a good photocatalytic performance and the BiFeO₃ nanoparticle has a better photocatalytic activity than the BiFeO₃ bulk. In addition, the effect of the addition of dopants and formation of hetero-junction on the photocatalytic activity was also evaluated. Examples of photocatalytic performances on BFO are also given in last section.

BFO is a newly emerging material for the photocatalytic application and may be a promising material for hydrogen generation under visible light due to its narrow band gap and high efficiency of charge separation. However, the mechanism of photocatalysis is still disputable due to the insufficient experimental data. Therefore the future work is recommended to focus on the following aspects: 1) to design and obtain a specific BFO with suitable band gap by doping or forming hetero-junction to improve the visible-light response; 2) to establish the correlation between the structure of BFO and the photocatalytic activity to better understand the separation mechanism of photo-generated electron and hole; 3) to design practical BFO-based photocatalytic hydrogen generation system.

ACKNOWLEDGEMENTS

This work is financially supported by the National Natural Science Foundation of China (No. 51372237) and International S&T Cooperation Program of China (No. 2013DFG52490).

REFERENCES

- [1] H. Balat and E. Krtay // *Int. J. Hydrogen Energy* **35** (2010) 7416.
- [2] A. Fujishima and K. Honda // *Nature* **238** (1972) 37.
- [3] X.Y. Yang, A. Wolcott, G.M. Wang, A. Sobo, R.C. Fitzmorris, F. Qian, J.Z. Zhang and Y. Li // *Nano Letters* **9** (2009) 2331.
- [4] A. Wolcott, W.A. Smith, T.R. Kuykendall, Y.P. Zhao and J.Z. Zhang // *Adv. Funct. Mater* **19** (2009) 1849.
- [5] Z. Zhang, M.F. Hossain and T. Takahashi // *Appl. Catalysis B: Environmental* **95** (2010) 423.
- [6] X. Wei, T.F. Xie, L.L. Peng, W. Fu, J.S. Chen, Q. Gao, G.Y. Hong and D.J. Wang // *J. Phys. Chem. C* **115** (2011) 8637.
- [7] H. Wu and Z. Zhang // *Int. J. Hydrogen Energy* **36** (2011) 13481.
- [8] H.-J. Choi and M. Kang // *Int. J. Hydrogen Energy* **32** (2007) 3841.
- [9] A.L. Linsebigler, G.Q. Lu and J.T. Yates // *Chem. Reviews* **95** (1995) 735.
- [10] A. Hagfeldt and M. Gratzel // *Chem. Reviews* **95** (1995) 49.
- [11] S.Y. Yang, L.W. Martin, S.J. Byrnes, T.E. Conry, S.R. Basu, D. Paran, L. Reichertz, J. Ihlefeld, C. Adamo, A. Melville, Y.H. Chu, C.H. Yang, J.L. Musfeldt, D.G. Schlom, J.W. Ager and R. Ramesh // *Appl. Phys. Lett* **95** (2009) 062909.
- [12] L.M. Campos, A. Tontcheva, S. Gnes, G. Sonmez, H. Neugebauer, N.S. Sariciftci and F. Wudl // *Chem. Mater.* **17** (2005) 4031.
- [13] P.S. Brody // *Solid. State. Commun.* **12** (1973) 673.
- [14] V.M. Fridkin, *Springer Series in Solid-State Sciences, vol. 9* (Springer, New York, 1979).
- [15] M. Ichiki, H. Furue, T. Kobayashi, R. Maeda, Y. Morikawa, T. Nakada and K. Nonaka // *Appl. Phys. Let.* **87** (2005) 222903.
- [16] M. Ichiki, Y. Morikawa and T. Nakada // *Jpn. J. Appl. Phys.* **41** (2002) 6993.
- [17] K.Nonaka, M. Akiyama, T. Hagio and A. Takase // *Jpn. J. Appl. Phys.* **34** (1995) 2344.

- [18] M. Qin, K. Yao, Y.C. Liang and S. Shannigrahi // *J. Appl. Phys.* **104** (2007) 014104.
- [19] F. Gao, X.Y. Chen, K.B. Yin, S. Dong, Z.F. Ren, F. Yuan, T. Yu, Z.G. Zou and J.M. Liu // *Adv. Mater.* **19** (2007) 2889.
- [20] Z. Zhang, H. Liu, Y. Lin, Y. Wei, C.-W. Nan and X. Deng // *J. Nanomaterials* **2012** (2012) 1.
- [21] S. Li, Y.H. Lin, B.P. Zhang, Y. Wang and C.W. Nan // *J. Phys. Chem. C* **114** (2010) 2903.
- [22] X. Xu, Y.-H. Lin, P. Li, L. Shu, C.-W. Nan and J. Ihlefeld // *J. Am. Ceram. Soc.* **94** (2011) 2296.
- [23] M.M. Rashad // *J. Materials Science-Materials in Electronics* **23** (2012) 882.
- [24] C.J. Tsai, C.Y. Yang, Y.C. Liao and Y.L. Chueh // *J. Mater. Chem.* **22** (2012) 17432.
- [25] Y.P. Wang, L. Zhou, M.F. Zhang, X.Y. Chen, J.M. Liu and Z.G. Liu // *Appl. Phys. Lett.* **84** (2004) 1731.
- [26] M.M. Kumar, V.R. Palkar, K. Srinivas and S.V. Suryanarayana // *Appl. Phys. Lett.* **76** (2000) 2764.
- [27] A.K. Pradhan, K. Zhang, D. Hunter, J.B. Dadson, G.B. Loiutts, P. Bhattacharya, R. Katiyar, J. Zhang, D.J. Sellmyer, U.N. Roy, Y. Cui and A. Burger // *J. Appl. Phys.* **97** (2005) 093903.
- [28] S.K. Singh, Y. Kim K, H. Funakubo and H. Ishiwara // *Appl. Phys. Lett.* **88** (2006) 162904.
- [29] D.-C. Jia, J.-H. Xu, H. Ke, W. Wang and Y. Zhou // *J. European Ceram. Soc.* **29** (2009) 3099.
- [30] S.H. Xie, J.Y. Li, R. Porksch, Y.M. Liu, Y.C. Zhou, Y.Y. Liu, Y. Ou, L.N. Lan and Y. Qiao // *Appl. Phys. Lett.* **93** (2008) 222904.
- [31] G.S. Arya and N.S. Negi // *J. Physics D-Applied Physics* **46** (2013) 1.
- [32] L. Zhai, Y.G. Shi, J.L. Gao, S.L. Tang and Y.W. Du // *J. Alloys and Compounds* **509** (2011) 7591.
- [33] X. Wang, Y. Lin, Z.C. Zhang and J.Y. Bian // *Journal of Sol-Gel Science and Technology* **60** (2011) 1.
- [34] X. Wang, Y. Lin, X.F. Ding and J.G. Jiang // *J. Alloys and Compounds* **509** (2011) 6585.
- [35] H. Yang, T. Xian, Z.Q. Wei, J.F. Dai, J.L. Jiang and W.J. Feng // *J. Sol-Gel Science and Technology* **58** (2011) 238.
- [36] H.P. Klug and L.E. Alexander, *X-ray Diffraction Procedures, 2d Edition* (Wiley, New York, 1974).
- [37] J.H. Peng, M. Hojamberdiev, B.W. Cao, J.A. Wang and Y.H. Xu // *Applied Physics a-Materials Science & Processing* **103** (2011) 511.
- [38] J.P. Zhou, R.L. Yang, R.J. Xiao, X.M. Chen and C.Y. Deng // *Mater. Res. Bull.* **47** (2012) 3630.
- [39] J.Z. Jiang, J. Zou, M.N. Anjum, J.C. Yan, L. Huang, Y.X. Zhang and J.F. Chen // *Solid State Sciences* **13** (2011) 1779.
- [40] S.H. Han, K.S. Kim, H.G. Kim, H.-G. Lee, H.-W. Kang, J.S. Kim and C.I. Cheon // *Ceram. Int.* **36** (2010) 1365.
- [41] B. Liu, B.B. Hu and Z.L. Du // *Chem. Commun.* **47** (2011) 8166.
- [42] F. Gao, Y. Yuan, K.F. Wang, X.Y. Chen, F. Chen and J.M. Liu // *Appl. Phys. Lett.* **89** (2006) 216.
- [43] X.Y. Zhang, C.W. Lai, X. Zhao, D.Y. Wang and J.Y. Dai // *Appl. Phys. Lett.* **87** (2005) 143102.
- [44] J. Wang, M.Y. Li, X.L. Liu, L. Pei, J. Liu, B.F. Yu and X.Z. Zhao // *Chinese Science Bulletin* **55** (2010) 1594.
- [45] U.A. Joshi, J.S. Jang, P.H. Borse and J.S. Lee // *Appl. Phys. Lett.* **92** (2008) 242106.
- [46] G.Q. Tan, Y.Q. Zheng, H.Y. Miao, A. Xia and H.J. Ren // *J. Am. Ceram. Soc.* **95** (2012) 280.
- [47] X.H. Zhu, Q.M. Hang, Z.B. Xing, Y. Yang, J.M. Zhu, Z.G. Liu, N.B. Ming, P. Zhou, Y. Song, Z.S. Li, T. Yu and Z.G. Zou // *J. Am. Ceram. Soc.* **94** (2011) 2688.
- [48] S. Komarneni, V.C. Menon, Q.H. Li, R. Roy and E. Ainger // *J. Am. Ceram. Soc.* **79** (1996) 1409.
- [49] C. Reitz, C. Suchomski, C. Weidmann and T. Brezesinski // *Nano Res.* **4** (2011) 414.
- [50] C. Hengky and S. Dunn // *MRS Proceedings* **1443** (2012)
- [51] C. Hengky, X. Moya, N.D. Mathur and S. Dunn // *RSC Adv.* **2** (2012) 11843.
- [52] L. Wang, J.-B. Xu, B. Gao, L. Bian and X.-Y. Chen // *Ceram. Int.* **39** (2013) S221.
- [53] W. Wang, N. Li, Y. Chi, Y. Li, W. Yan, X. Li and C. Shao // *Ceram. Int.* **39** (2013) 3511.
- [54] J. Yang, X. Li, J. Zhou, Y. Tang, Y. Zhang and Y. Li // *J. Alloys and Compounds* **509** (2011) 9271.

- [55] L. Fei, J. Yuan, Y. Hu, C. Wu, J. Wang and Y. Wang // *Crystal Growth & Design* **11** (2011) 1049.
- [56] A. Kudo, H. Kato and I. Tsuji // *Chem. Lett.* **33** (2004) 1534.
- [57] T. Choi, S. Lee, Y.J. Choi, V. Kiryukhin and S.W. Cheong // *Science* **324** (2009) 63-66.
- [58] A.B. Murphy, P.R.F. Barnes, L.K. Randeniya, I.C. Plumb, I.E. Grey, M.D. Horne and J.A. Glasscock // *Int. J. Hydrogen Energy* **31** (2006) 1999.
- [59] J. He, R. Guo, L. Fang, W. Dong, F. Zheng and M. Shen // *Mater. Res. Bull.* (2013) 58.
- [60] Y. Liu, R. Zuo and S. Qi // *J. Molecular Catalysis A: Chemical.* **376** (2013) 1.
- [61] K.A. McDonnell, N. Wadnerkar, N.J. English, M. Rahman and D. Dowling // *Chem. Phys. Lett.* **572** (2013) 78.
- [62] T. Soltani and M.H. Entezari // *Ultrasonics Sonochemistry* **20** (2013) 1245.
- [63] J. Deng, S. Banerjee, S.K. Mohapatra, Y.R. Smith and M. Misra // *J. Fundamentals of Renewable Energy and Applications* **1** (2011) 1.
- [64] T. Soltani and M.H. Entezari // *Chemical Engineering Journal* **223** (2013) 145.
- [65] S. Banerjee, S.K. Mohapatra and M. Misra // *Chem. Commun.* **46** (2009) 7137.
- [66] S.K. Mohapatra, S.E. John, S. Banerjee and M. Misra // *Chem. Mater.* **21** (2009) 3048.
- [67] K.S. Rajeswar, R. McConnell and S. Litch, *Solar Hydrogen Generation: Toward a Renewable Energy Future* (Springer, NewYork, 2008).
- [68] Z.G. Zou, J.H. Ye, K. Sayama and H. Arakawa // *Nature* **414** (2001) 625.
- [69] Q.Y. Li and G.X. Lu // *J. Mol. Catal. A: Chem.* **266** (2007) 75.
- [70] V.M. Fridkin // *Crystallography Reports* **46** (2001) 722.
- [71] W. Ji, K. Yao and Y.C. Liang // *Adv. Mater.* **22** (2010) 1763.
- [72] R. Moubah, O. Rousseau, D. Colson, A. Artemenko, M. Maglione and M. Viret // *Adv. Funct. Mater.* **22** (2012) 4814.
- [73] H.T. Yi, T. Choi, H.-J. Choi, Y.S. Oh and S.W. Cheong // *Adv. Mater.* **23** (2011) 3403.
- [74] D. Cai, D. Du, S. Yu and J. Cheng // *Procedia Engineering* **27** (2012) 577.
- [75] X. Zhang, J. Lv, L. Bourgeois, J. Cui, Y. Wu, H. Wang and P.A. Webley // *New Journal of Chemistry* **35** (2011) 937.
- [76] S. Mukherjee, S. Chakraborty and S. Mukherjee // *Int. J. Current Engineering and Technology* **12** (2012) 403.
- [77] M.B. Bellakki and V. Manivannan // *J. Sol-Gel Science and Technology* **53** (2010) 184.
- [78] Z. Zhang, H. Liu, Y. Lin, Y. Wei, C.-W. Nan and X. Deng // *J. Nanomaterials* **2012** (2012) 1.
- [79] A. Mukherjee, S.M. Hossain, M. Pal and S. Basu // *Applied Nanoscience* **2** (2012) 305.
- [80] M. Ge, Y.F. Li, L. Liu, Z. Zhou and W. Chen // *J. Phys. Chem. C* **115** (2011) 5220.
- [81] J.Z. Su, L.J. Guo, N.Z. Bao and C.A. Grimes // *Nano Lett.* **11** (2011) 1928.
- [82] X. Wei, T.F. Xie, L.L. Peng, W. Fu, J.S. Chen, Q. Gao, G.Y. Hong and D.J. Wang // *J. Phys. Chem. C* **115** (2011) 8637.
- [83] K. Sivula, F. Le Formal and M. Gratzel // *Chem. Mater.* **21** (2009) 2862.
- [84] R. Guo, L. Fang, W. Dong, F. Zheng and M. Shen // *J. Mater. Chem.* **21** (2011) 18645.
- [85] T. Li, J. Shen, N. Li and M. Ye // *Mater. Lett.* **91** (2013) 42.